Electrical Power and Energy Systems 156 (2024) 109708

Contents lists available at ScienceDirect

International Journal of Electrical Power and Energy Systems

journal homepage: www.elsevier.com/locate/ijepes

Optimal single settings based relay coordination in DC microgrids for line faults

Sunil Kumar Maurya *, Atul Kumar Soni, Abheejeet Mohapatra, Ankush Sharma

Department of Electrical Engineering, Indian Institute of Technology Kanpur, India

ARTICLE INFO

Keywords:
DC microgrid
Inverse characteristics
Line current rise rate
Primary relay
Backup relay
Pole-to-ground fault
Pole-to-pole fault
Relay coordination

ABSTRACT

A novel time–current-rate-based inverse characteristic curve for relays in a DC microgrid is proposed in this paper. Line current rise rate is used as actuating quantity, ensuring quick line fault clearing (relay operating time is in order of a few μs). The advantage of using line current rise rate as actuating quantity is that for a line short-circuit fault, it does not vary significantly for grid-connected and islanded modes of operation and varying network topologies of DC microgrid. Consequently, using the proposed characteristic, a single set of optimal relay settings is obtained using an optimization solver in MATLAB. The obtained settings ensure reliable and selective coordination between primary and backup relays for various pole-to-ground and pole-to-pole line faults under different operating conditions with multiple sources in two different 4-bus 400V low voltage DC microgrids. The maximum relay operating time for a high resistance fault with the proposed curve is 394.9 μs for the first considered low voltage DC microgrid. Simulations in the Real Time Digital Simulator and comparisons with previous schemes (one comparison on the second considered DC microgrid), conventional standard inverse, and extremely inverse curves for DC microgrid protection indicate the effectiveness of the proposed scheme.

Abbreviations

BESS	Battery Energy Storage Systems
CBs	Circuit Breakers
CTI	Coordination Time-Interval
EI	Extremely Inverse
GC	Grid-Connected
HRF	High Resistance Fault
LVDC	Low Voltage DC
NLP	Non-Linear Programming
PG	Pole-to-Ground
PP	Pole-to-Pole
PV	Photo-Voltaic
RTDS	Real-Time Digital Simulator
SI	Standard Inverse

1. Introduction

The ease of integration of solar Photo-Voltaic (PV) and Battery Energy Storage Systems (BESSs) based renewable energy resources in a DC microgrid, compared to an AC microgrid, has led to the increased expansion and research interest of DC microgrids over AC microgrids [1,2]. Also, DC microgrid can be a great way to power remote towns, shipboards, spaceships, and grids with sensitive loads, where the quality of power is crucial [3,4]. However, the rate of rise of current is very high in a DC microgrid during a line fault due to the rapid discharge of the DC link capacitor and the associated low line impedance [5]. Hence, in general, the DC microgrid protection schemes follow a three-time frame based protection methodology in which the protection of the line, feeder, and the source should be done within a few μs, milliseconds, and seconds, respectively [6]. Several DC Circuit Breakers (CBs) have been developed to support the quick isolation of lines during a fault in a DC microgrid, among which the solid-state CBs have a response time in the range of a few μs [7,8].

1.1. Motivation

Consider the radial DC microgrid shown in Fig. 1. For a fault in $Line_2$, the upstream relay R_1 may sense a fault current similar to the fault current sensed by the primary relay R_2 due to the short line length, low network impedance, and high fault current as compared to the load

* Corresponding author.
E-mail addresses: suniliitk20@iitk.ac.in (S.K. Maurya), atulsoni@iitk.ac.in (A.K. Soni), abheem@iitk.ac.in (A. Mohapatra), ansharma@iitk.ac.in (A. Sharma).

https://doi.org/10.1016/j.ijepes.2023.109708
Received 26 July 2023; Received in revised form 8 November 2023; Accepted 4 December 2023
Available online 8 December 2023

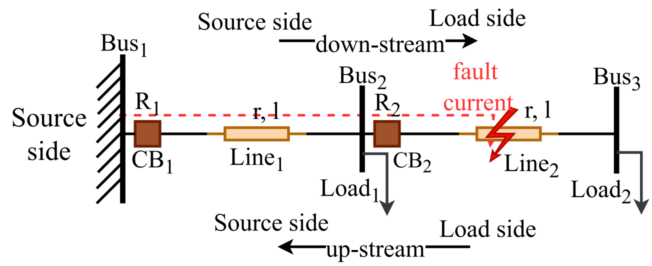

Fig. 1. Illustration of a line fault in a radial DC microgrid.

current. Hence, without proper coordination, there is a possibility that the trip times of relays R_1 and R_2 are similar for the fault in Line$_2$. This uncoordinated operation of relays and associated solid-state CBs during a line fault in DC microgrid will lead to unnecessary load isolation and possible blackout.

To ensure minimal load isolation and avoid possible blackout during a fault, proper selectivity is needed between the primary and upstream relays, which consequently trip the associated solid-state CBs. Appropriate selectivity between them can be achieved by coordinating their operation times. Further, the upstream relay, such as R_1 in Fig. 1, should provide backup to primary relay R_2 for a fault on Line$_2$ to enhance the system's reliability. In addition, due to very high rate of current rise in DC microgrid, the operating time of primary relay should be within a few μs while ensuring the required selectivity with upstream relays. The need to consider the above aspects and develop a solution to the issues associated with relay coordination in a DC microgrid is the primary motivation of the research work in this paper.

1.2. Literature review

Several techniques to coordinate relays in DC microgrid exist in literature, which can be categorized as interlocking-based techniques, online fault location estimation techniques, and time–current characteristic-based techniques. Table 1 shows the different attributes of these techniques. In [9,10], adjustable time–current settings are used to identify primary and backup (upstream) relays for a line fault. Further, using communication, a signal is used to block possible undesired operation of backup relay. For each relay, a two-stage over-current characteristic (primary and backup) is suggested in [9]. However, such techniques require a dedicated fast communication link. Any delay in the signal or link failure may undermine the coordination between the primary relay and the upstream relay.

In a DC microgrid, relays can also be coordinated by identifying primary and backup zones of relay via online fault location estimation. In [11], the first and second current rise rates are used to estimate line inductance up to fault point and fault resistance, respectively. [12] suggests placing an additional relay near the main relay to estimate fault location using relative voltage drop between relays. However, due to approximations in the line inductance estimation and small line lengths of DC microgrid, the accuracy of [11,12] reduces with an increase in fault resistance. The error in inductance estimation in [12] can be reduced by more calculations, which significantly increase the relay's operating time. In [13], local measurements of bus voltage, line current, and line current rise rate are used to determine the line inductance, which is then compared with the defined protection zones to coordinate relays. The inductance-based protection zone division's selectivity may reduce for different network configurations. Also, it can be observed from Table 1 that [11–13] are not analyzed for different network configurations and modes of operations of DC microgrid.

Apart from interlocking and fault location based techniques, very few time–current characteristic-based techniques exist in the literature to uphold the desired selectivity between the primary and upstream relays in the DC microgrid. In [14], a unique control circuit with a time–current curve is used to coordinate the relays. However, the considered characteristics curve is not thoroughly discussed. An instantaneous tripping strategy is suggested in [15] for Low Resistance Fault (LRF) in lines of DC microgrid, which, however, may lead to unnecessary isolation in a large network. [16] presents a short-circuit and an instantaneous time–current profile for relay coordination in DC microgrid, depending on the magnitude of fault current. However, for short-circuit time–current profile, the dial setting with time in range of μs is used, which may undermine the significance of other parameters of the used curve. A current derivative-based factor is suggested in [17] to coordinate relays with low operating time. However, [16,17] are not analyzed for different network configurations, modes of operation, and multiple source injections in the DC microgrid.

It can be observed from the literature review that the reliability of interlocking-based techniques primarily depends on the communication link's data rate transfer capability. Also, interlocking-based techniques require a non-communication-based backup relay coordination technique during communication link failure. The online fault location estimation-based relay coordination techniques also have reliability issues due to possible over or under reach, explicitly with increased fault resistance concerning the small line lengths in the DC microgrid [11]. The previous standard time–current characteristic based relay coordination approaches have relay operating times (fault clearing times) in the order of few tens to thousands of μs, as given in Table 1. However, these techniques are not thoroughly analyzed for different network configurations and modes of operation of the DC microgrid. Hence, an approach is needed for relay coordination in DC microgrids, which supports the quick relay operating (fault clearing) time and maintains appropriate selectivity and reliability between the primary and backup relays for different network configurations and modes of operations of the DC microgrid.

1.3. Contribution and paper structure

This paper proposes a novel time–current-rate based inverse characteristic curve for the relays in a DC microgrid, which uses the line current rise rate as an actuating quantity and ensures quick clearing of line faults (relay operating time is in order of few μs). In the proposed work, optimal values of the characteristic constants in the standard IEC/IEEE family of curves [18,19] are obtained in addition to the plug setting and time multiplier setting of the relays by solving a Non-Linear Programming (NLP) problem, which ensure quick clearing of line faults in a DC microgrid. The benefit of using line current rise rate as an actuating quantity is that, for a line short-circuit fault, it does not vary significantly for a relay due to intermittency of generation from renewable energy sources, Grid-Connected (GC) and islanded modes of operation and different ring and radial topologies of the DC microgrid [20]. Hence, using the proposed characteristic curve, a single set of optimal settings for each relay is obtained, which ensures reliable and selective coordination between primary and upstream relays for different line short-circuit faults under different operating conditions with multiple sources in a Low Voltage DC (LVDC) microgrid. The optimal relay settings are obtained in MATLAB using an optimization solver. The proposed scheme can coordinate relays with non-unit line fault detection schemes, such as [21,22], or act as a backup for relays with communication-based method. The efficacy of proposed scheme is validated via Real-Time Digital Simulator (RTDS) based simulations and comparisons with [16,17], and conventional Standard Inverse (SI) as well as Extremely Inverse (EI) relay characteristic curves for DC microgrid protection.

The rest of the paper is structured as follows. Section 2 discusses the NLP-based relay coordination problem in DC microgrids and the proposed technique to obtain single settings of novel time–current-rate based characteristic curve for all relays. The associated simulation results are discussed in Section 3. Comparative analysis and associated discussion are given in Section 4, while Section 5 concludes the paper.

Table 1
Comparison of proposed method with previous methods (✓: satisfies, ✗: fails, –: not-reported/untested).

Reference	Type of coordination technique	Technique	Maximum operating time of primary relay for LRF	Grid-connected /Islanded	Ring/ Radial topology	Multiple sources considered	Online update of settings not required
[9]	Interlocking	Communication assisted two zone based over-current scheme	1 ms	✓/✓	–/✓	✓	✗
[10]		Communication assisted over-current scheme	1 ms	–/✓	✓/–	✓	✗
[11]	Online fault location	Inductance based fault location estimation using di/dt and d^2i/dt^2	–	✓/–	–/✓	✓	✓
[12]		Online fault distance evaluation using voltage of two relay points	51.36 ms	✓/–	–/✓	✗	✓
[13]		Equivalent inductance estimation using local signals	< 1 ms	✓/–	–/✓	✗	✓
[14]	Time–current curve	Time–current curve with unique mixed-signal control circuit	≈ 29 μs	✓/–	✓/–	✓	✓
[15]		Instantaneous tripping	–	–/✓	–/✓	✗	✓
[16]		Modified curve of time and current	170 μs	✓/–	–/✓	✓	✓
[17]		di/dt assisted protection coordination	3 ms	✓/–	–/✓	✗	✓
Proposed		Unique characteristic curve using di/dt as actuating quantity	84.9 μs	✓/✓	✓/✓	✓	✓

2. Proposed relay coordination formulation and novel relay characteristics

The basic relay coordination problem for DC microgrids is formulated first, followed by the proposed novel characteristic curve for numerical relay coordination in DC microgrid. To obtain the novel relay characteristic curve, the line current rise rate is used as actuating quantity as it mostly remains unaffected during a fault for GC and islanded modes of operation, and different ring and radial topologies of DC microgrid [20]. Further, as per [21], the effect of noise is insignificant in the line current rise rate due to the very high magnitude of the latter during a fault, as compared to line current. Further, commercial industry-grade numerical relays for DC microgrid protection can accurately estimate the line current rise rate with very good immunity to measurement noise [23]. Using the proposed relay characteristic curve, unique values of TMS and PS for each relay, and two additional characteristic constants are obtained by solving the relay coordination problem formulated as a Non-Linear Programming (NLP) problem. The unique relay settings ensure quick fault clearing (relay operating time is in order of few μs) and reliable and selective coordination between primary and upstream relays for different line faults under different operating conditions with multiple sources in a DC microgrid.

2.1. Relay coordination formulation

The coordination of time–current characteristic-based relays is generally formulated as a constrained optimization problem. The sum of operating times of primary relays is commonly chosen as the objective (z) [24], which is minimized as

$$z = \min \sum_{i=1}^{N} t_{pr,o_i} \tag{1}$$

where t_{pr,o_i} is the operating time of the primary relay R_i, and N is the total number of relays. As per the standard IEC/IEEE family of curves [18,19], t_{pr,o_i} can be stated as

$$t_{pr,o_i} = TMS_i \left(\frac{A}{\left(\frac{\alpha_{iL}}{PS_i}\right)^{\gamma} - 1} + B \right), \forall i \tag{2}$$

where A, B, and γ are characteristic constants, and α_{iL} is the instantaneous value of the actuating quantity sensed by relay R_i for a fault that has occurred at location L. TMS_i and PS_i are the respective TMS and PS of R_i. α_{iL}/PS_i in (2) is often also known as Plug Multiplier Setting (PMS_i). Please note that an expression similar to (2) is also true for t_{ba,o_j} $\forall j$, the operating time of associated backup relay R_j.

The coordination problem has constraints due to limitations on relay operating time, settings, and selectivity required between backup and primary relays. The operating time of a relay is a function of its characteristic constants, TMS_i, PS_i, and instantaneous value of actuating quantity as given in (2). Further, t_{pr,o_i} is usually bounded as

$$t_{o_i}^{\min} \le t_{pr,o_i} \le t_{o_i}^{\max}, \forall i \tag{3}$$

where, $t_{o_i}^{\min}$ and $t_{o_i}^{\max}$ are respective minimum and maximum bounds of operating time of R_i. The operating time of the associated backup relay R_j is also bounded by a constraint similar to (3). TMS_i and PS_i of relay R_i are bounded as

$$TMS_i^{min} \le TMS_i \le TMS_i^{max}, \forall i \tag{4}$$

$$PS_i^{min} \le PS_i \le PS_i^{max}, \forall i \tag{5}$$

where, TMS_i^{min}, PS_i^{min} and TMS_i^{max}, PS_i^{max} represent the respective minimum and maximum bounds. Please note that (4) and (5) are also true for backup relay R_j. Considering the advancement in numeric relays, TMS_i and PS_i can have any continuous value between the bounds defined by the manufacturer. A sensible regulation of PS_i can help in maintaining the appropriate selectivity without having dependability issues, especially for different network configurations and modes of operations of DC microgrid [25].

For minimum load isolation during a fault, the operating time of backup relay R_j, i.e., t_{ba,o_j}, must be more than t_{pr,o_i} corresponding to primary relay R_i. In fact, a minimum time margin, called as Coordination Time-Interval (CTI), is maintained between the operating times of $R_i - R_j$ pair as

$$t_{ba,o_j} - t_{pr,o_i} \ge CTI, \forall (i,j) \tag{6}$$

For selectivity between relay pairs R_i and R_j, CTI is defined based on operation time of associated solid-state CBs, possible delays, and additional safety margins [16].

2.2. Proposed technique

The process of obtaining the proposed novel relay characteristic curve for LVDC microgrid protection against line faults is discussed here. The first novelty of the proposed relay characteristic curve is that unique values of TMS_i and PS_i for each relay R_i, and one set of common values of A and γ for all relays are obtained. The settings are determined by considering various Pole-to-Ground (PG), Pole-to-Pole (PP) LRFs, and PG High Resistance Faults (HRFs) in lines of LVDC microgrid for different modes of operation, network configurations, and given peak load at each bus, by solving a NLP problem with objective as

$$z = \min \sum_{m=1}^{M} \sum_{i=1}^{N} t_{pr,o_{i,m}} \tag{7}$$

where $t_{pr,o_{i,m}}$ is the operating time of primary relay R_i for the mth scenario. Please note that (7) is the modified form of (1), where M is the total number of PG, PP line fault scenarios considered for R_i subject to different network configurations, modes of operation, and fault resistances. More details in this regard are provided in Sections 3.2 and 3.3. Consequently, (2) is modified as,

$$t_{pr,o_{i,m}} = TMS_i \left(\frac{A}{\left(\frac{\alpha_{iL,m}}{PS_i}\right)^{\gamma} - 1} + B \right), \forall i, \forall m \in M \tag{8}$$

where $\alpha_{iL,m}$ is the actuating quantity sensed by R_i for a fault at location L in the mth scenario. B in (8), for all relays, is chosen as zero to avoid unnecessary delay in relay operation. Please note similar to (2), (8) is also true for the associated backup relay operating time in the mth scenario. Thus, A and γ in (8) are two additional variables along with TMS_i and PS_i variables for each relay R_i in DC microgrid for the proposed NLP problem. Issues with not using Standard Inverse (SI) and Extremely Inverse (EI) relay characteristics for DC microgrid protection, as compared to proposed relay characteristics, are discussed in Section 4.2.

The second novelty of the proposed characteristic is that the line current rise rate sensed by relay R_i is used as actuating quantity, i.e., $\alpha_{iL,m}$, in (8), owing to its significantly high value during a line fault in DC microgrid and robustness to different network configurations and modes of operations [20]. The issues with not using line current magnitude as an actuating quantity in (2) with respect to the proposed characteristics are explained in Section 4.3.

Similar to (8), (3) and (6) are, respectively, modified as

$$t_{o_i}^{\min} \le t_{pr,o_{i,m}} \le t_{o_i}^{\max}, \forall i, \forall m \in M \tag{9}$$

$$t_{ba,o_{j,m}} - t_{pr,o_{i,m}} \ge CTI, \forall (i,j), \forall m \in M \tag{10}$$

Constraint on TMS_i in (4) is considered in the NLP problem. PS_i^{min} and PS_i^{max} in (5) are evaluated as [25,26]

$$PS_i^{min} = min\left(SF \times I_{rr_i}^{nom}, I_{rr,f_i}^{min}\right), \forall i \tag{11}$$

$$PS_i^{max} = max\left(2 \times I_{rr_i}^{nom}, I_{rr,f_i}^{max}\right), \forall i \tag{12}$$

where SF is safety factor to account for any unseen increase in line current rise rate, i.e., I_{rr_i}. $I_{rr_i}^{nom}$ is nominal value of I_{rr_i}, and I_{rr,f_i}^{min} (I_{rr,f_i}^{max}) is the minimum (maximum) I_{rr_i} sensed by R_i for all PG, PP LRFs, and PG HRFs with different modes of operation, network configurations, and given peak load at each bus (details are in Sections 3.2 and 3.3). PS_i^{min} in (11) provides appropriate security by avoiding possible maloperation of relay R_i. PS_i^{max} in (12) defines the sensitivity of R_i. Additional bounds on A and γ are considered to have a bounded NLP problem as,

$$A^{min} \le A \le A^{max} \tag{13}$$

$$\gamma^{min} \le \gamma \le \gamma^{max} \tag{14}$$

where A^{min} and A^{max} (γ^{min} and γ^{max}) are the minimum and maximum bounds on A (γ) in (8), respectively. More details on the considered bounds in (4), (5), (9), (10), (13), and (14) are discussed in Section 3.2.

The solution of the formulated NLP-based proposed relay coordination problem, i.e., (4), (5), (7)–(14), for LVDC microgrids, considering all operating conditions stated above, is obtained using MATLAB-based solver $fmincon$. The obtained solution is a local minima, which gives

Table 2
Relay pairs (RPs) for system in Fig. 2.

RPs	1	2	3	4	5	6	7	8
Primary relay	R_1	R_2	R_3	R_4	R_5	R_6	R_7	R_8
Backup relay	R_7	R_4	R_1	R_6	R_3	R_8	R_5	R_2

optimized values of A and γ in (8), common to each relay, and unique TMS_i and PS_i for each relay. It is observed from the results (discussed next) that the novel relay characteristic curve, based on optimized values of A and γ, can effectively coordinate the relays with the obtained settings while meeting the quick line fault isolation (in a few µs) requirement of a LVDC microgrid.

It is to be noted that the proposed scheme requires a non-unit line fault detection scheme, such as [21,22], as a precursor to detect forward line fault. The precursor line fault detection scheme also takes care of the segregation of line faults from non-fault transients, such as load and source switching.

3. Simulation results and obtained settings

3.1. Test system

The considered test system is a 4-bus 400V LVDC microgrid, as shown in Fig. 2. It has two internal sources (12 kW solar PV source and BESS), each to fulfill their local loads [27]. Solar PV source and BESS are integrated via DC/DC boost and synchronous bi-directional converters [28]. The considered system can be set up in ring or radial network topology and can be operated in GC or islanded mode via operation of solid-state CBs. The system is connected to AC grid via AC/DC bi-directional converter [29], which can operate in inverter or rectifier mode, as per system requirement. Further details of the test system are in [22].

The test system in Fig. 2 is modeled in RTDS with a sampling time of 60 µs. 400 V (nominal system voltage) and 75 A (total load) nominal line current are considered as base. Considering potential bidirectional power flow, eight relays are required to ensure complete line short-circuit protection, as shown in Fig. 2 and listed in Table 2. The relays in Fig. 2 are not inherently directional. However, using the precursor technique [21,22], they are sensitive only to forward faults and restrain for backward faults. A detailed steady-state and fault analysis is performed for each relay in Fig. 2, which aids in obtaining constraints‘ bounds, as discussed next.

3.2. Determination of variables' bounds

Considering the possible ring, radial network configurations, and GC, islanded modes of operations of system in Fig. 2, the nominal line current rise rate, i.e., $I_{rr_i}^{nom}$ in (11) and (12), is 53.33 pu/s for all relays in Fig. 2. The process to evaluate $I_{rr_i}^{nom}$ is as follows. As per [23], the line current rise rate is analyzed for each line in Fig. 2 in RTDS for ring, radial network configurations, and GC, islanded modes of operation with peak load at each bus. Taking into account the different steady-state cases and small load changes (≤ 1 kW), the maximum line current rise rate for all lines in Fig. 2 is in range of $[2000, 3000]$A/s. Hence, considering additional safety margin and as per [21], $I_{rr_i}^{nom}$ is 4000 A/s (53.33 = 4000/75 pu/s, where 75 A is base current) for each relay in Fig. 2. Further, PS_i^{min} and PS_i^{max} in (11) and (12) are determined by performing a comprehensive PG and PP LRFs, and PG HRFs analysis for GC, islanded modes of operation, and ring, radial configuration of system in Fig. 2, as given in Tables 3 and 4.

As per [30], a PP fault is generally a LRF in LVDC microgrid whereas a PG fault can either be a LRF or HRF. For islanded mode of operation, solid-state breaker CB_{isl} in Fig. 2 is intentionally opened. Similarly,

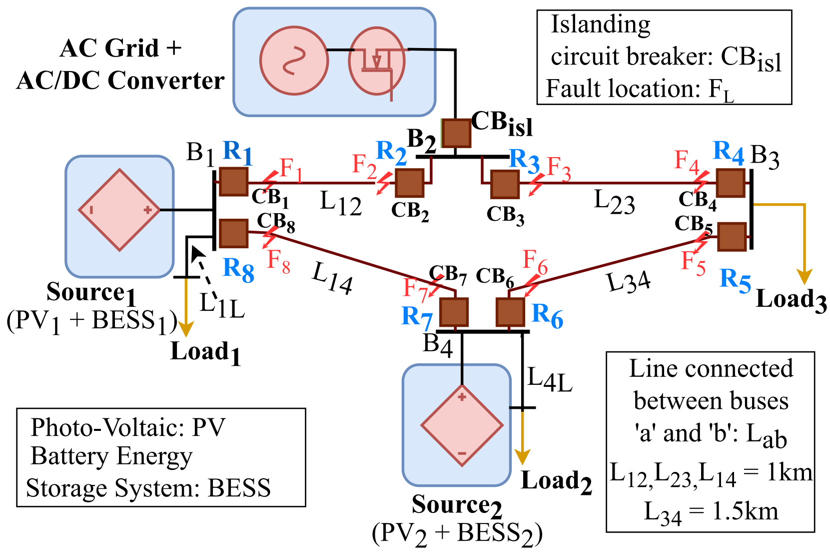

Fig. 2. 400V 4-bus LVDC microgrid [22] simulated in RTDS.

Table 3
Line current rise rate in pu/s sensed by relays in Table 2 during PG fault with R_f = 0.01(20) Ω at different locations F_L in Fig. 2.

F_L	RPs	Ring				Radial	
		GC		Islanded			
		$I_{rr,f_{iL}}$	$I_{rr,f_{jL}}$	$I_{rr,f_{iL}}$	$I_{rr,f_{jL}}$	$I_{rr,f_{iL}}$	$I_{rr,f_{jL}}$
F_1	1	9000.0 (2153.1)	2744.0 (658.2)	8852.0 (2233.5)	2572.9 (649.5)	–	–
	2	2730.5 (655.6)	860.4 (258.0)	2017.4 (509.3)	827.3 (279.7)	3495.5 (1134.8)	2986 (955.3)
F_2	1	4216.9 (1127.4)	937.13 (273.9)	4262.7 (1238.7)	804.2 (264.4)	–	–
	2	5516.9 (1473.3)	2855.1 (762.8)	4055.4 (1178)	2499.9 (726.4)	5821.1 (1623.8)	3211.6 (938.8)
F_3	3	6330.7 (1720)	3773.3 (1027.5)	5293.1 (1554.1)	3879.7 (1139.2)	5734.2 (1574.2)	3095.8 (851.0)
	4	3180.7 (866.1)	1426.7 (433.9)	2724.3 (799.5)	1721.8 (583.3)	3505 (961.3)	2347.9 (707.8)
F_4	3	3273.3 (893.3)	1821.3 (564)	2958.4 (877.3)	2359.6 (804.0)	3406.5 (929.8)	2245 (689.2)
	4	6086.7 (1660)	2841.2 (774.5)	4943 (1465.6)	3040.7 (901.5)	6015.9 (1643.2)	2727.4 (745.0)
F_5	5	6617.2 (1797.3)	2933.3 (797.3)	5035.2 (1504.3)	2672.5 (798.2)	6706.2 (1844.7)	3085.4 (917.1)
	6	3231.6 (877.3)	740 (222.7)	3325.8 (993.6)	565.4 (190.1)	–	–
F_6	5	2533.1 (646.4)	813.5 (242.7)	2049 (533.5)	609.3 (202.1)	3324.7 (1205.4)	2909.6 (953.1)
	6	8637.3 (2200)	3273.9 (835.2)	8529.6 (2220.8)	3064.2 (798.2)	–	–
F_7	7	7190.5 (1812.5)	2114.5 (533.0)	6895.4 (1774.2)	1678.4 (431.9)	–	–
	8	3806.6 (959.6)	582.3 (127.5)	3601 (926.8)	311.5 (147.5)	–	–
F_8	7	3300.8 (794.1)	305.9 (93.3)	3153.1 (779.8)	220.9 (127.1)	–	–
	8	8533.3 (2052.8)	2257.6 (542.9)	8077.8 (1997.6)	1621.9 (401.2)	–	–

to operate the system in radial configuration, line L_{14} is made non-operational by opening breakers CB_7 and CB_8. It is worth mentioning that this case of radial configuration can also be considered as a line removal case. The removal of L_{14} reduces the number of relay pairs as relays R_7 and R_8 become redundant. Hence, the results for relevant relay pairs are not shown for radial configuration in Tables 3 and 4. Moreover, it should be noted that, in Fig. 2, other line (i.e., L_{12}, L_{23}, L_{34}) switchings can result in radial configuration. However, it is observed that similar line current rise rates or lower values are obtained, and hence, results for only one radial case are given in Tables 3 and 4.

For a given fault resistance, line current rise rate is comparatively high for close-in (= 10% of line length) and lower for line-end (= 90% of line length) PG/PP faults due to the respective low and high line impedances. Hence, using close-in, line-end PG, PP LRFs with fault resistance R_f = 0.01 Ω, and PG HRF with R_f = 20 Ω at different fault locations in Fig. 2, the line current rise rates sensed by each relay (pair wise) are given in Tables 3 and 4, respectively ($I_{rr,f_{iL}}$ and $I_{rr,f_{jL}}$ are the respective line current rise rates for fault at F_L sensed by primary relay R_i and backup relay R_j, respectively). The associated $I^{max}_{rr,f_{iL}}$ and $I^{min}_{rr,f_{iL}}$ in (11) and (12), obtained from Tables 3 and 4, are shown in Table 5.

Substituting $I^{nom}_{rr_i}$ = 53.33pu/s, and I^{min}_{rr,f_i}, I^{max}_{rr,f_i} from Table 5, and using SF = 1.25 in (11), (12), the obtained bounds on PS_i in (5) for each relay in Fig. 2 are given in Table 6. TMS^{min}_i and TMS^{max}_i in (4) for all relays are chosen as 0.01s and 1s, respectively. $t^{min}_{o_i}$ and $t^{max}_{o_i}$ in (9), for all relays are 1 μs and 5 ms, respectively, so that the proposed scheme can effectively meet the requirement of quick line fault clearing during a fault in LVDC microgrid besides the fault detection time (of the order of a few μs) by the precursor technique in [21,22]. Additionally, considering the operating time of the available solid-state CBs [7,8], and adequate safety margin to avoid misoperation due to unknown delay, CTI in (10) is chosen as 50 μs [16] for all relay pairs in Table 2. The chosen CTI aids in maintaining appropriate coordination between the operations of primary and backup relays. The bounds on A and γ in (13) and (14) are chosen as [0.01, 1] and [0.001, 2], respectively. It is to be noted that A^{min} is chosen to be greater than 0 in (13) to avoid instantaneous relay operation, which may cause coordination issues. γ^{min} is chosen to be greater than 0 in (14) to result in positive relay operating times in (8), consequently, also avoiding setting negative A^{min} and γ^{min}. Lastly, for $A^{max} \geq 1$ and $\gamma^{max} \geq 2$, the optimal relay settings do not change significantly, as observed next.

Table 4
Line current rise rate in pu/s sensed by relays in Table 2 during PP fault with $R_f = 0.01\ \Omega$ at different locations F_L in Fig. 2.

F_L	RPs	Ring				Radial	
		GC		Islanded			
		$I_{rr,f_{iL}}$	$I_{rr,f_{jL}}$	$I_{rr,f_{iL}}$	$I_{rr,f_{jL}}$	$I_{rr,f_{iL}}$	$I_{rr,f_{jL}}$
F_1	1	7701.2	3056.6	7677.9	1402.5	–	–
	2	2145.9	2010.4	1509.7	1402.5	4030.0	3948.8
F_2	1	3998.2	1250.9	3961.5	957.3	–	–
	2	3923.4	3340.2	2901.3	2423.2	4189.4	4186.7
F_3	3	4186.3	3935.9	3721.6	3905.2	3852.1	3070.9
	4	3367.9	1408.6	2431.3	1948.6	4106.9	2239.6
F_4	3	2587.0	2472.3	2490.6	2693.9	2856.2	2778.9
	4	6099.2	2914.2	3927.7	3029.9	6048.2	2602.2
F_5	5	6142.5	2550.8	3822.2	2461.8	6253.2	3007.1
	6	2980.2	739.1	3077.9	650.3	–	–
F_6	5	2478.8	427.9	1568.5	782.2	4395.1	2565.3
	6	7407.0	3371.4	7371.9	2968.2	–	–
F_7	7	6704.5	2437.0	6363.5	1355.1	–	–
	8	3363.4	397.7	2944.3	120.6	–	–
F_8	7	3267.1	303.13	2599.2	94.67	–	–
	8	8446.2	2235.0	6900.6	1169.9	–	–

Table 5
$I^{min}_{rr,f_{iL}}$ and $I^{max}_{rr,f_{iL}}$ in pu/s sensed by relay R_i in Fig. 2 from Table 3 and Table 4.

R_i	I^{min}_{rr,f_i}	I^{max}_{rr,f_i}	R_i	I^{min}_{rr,f_i}	I^{max}_{rr,f_i}
R_1	564	9000	R_5	93.29	6706.2
R_2	127.46	5821.1	R_6	433.92	8637.33
R_3	242.67	6330.67	R_7	273.867	7190.53
R_4	258.03	6099.2	R_8	222.67	8533.33

Table 6
Obtained bounds on PS_i for each relay in Fig. 2.

R_i	PS^{min}_i	PS^{max}_i	R_i	PS^{min}_i	PS^{max}_i
R_1	66.66	9000	R_5	66.66	6706.2
R_2	66.66	5821.1	R_6	66.66	8637.33
R_3	66.66	6330.67	R_7	66.66	7190.53
R_4	66.66	6099.2	R_8	66.66	8533.33

Table 7
Notations representing different faults under different network topologies and modes of operations of system in Fig. 2, as in Table 3 and Table 4.

	PG LRF	PP LRF	PG HRF
Ring, GC	aa	ab	ac
Ring, Islanded	ad	ae	af
Radial, GC	ag	ah	ai

Table 8
Obtained optimal settings of relays in Fig. 2 for the proposed curve.

R_i	TMS_i(s)	PS_i	R_i	TMS_i(s)	PS_i
R_1	0.6827	106.17	R_5	0.1476	148.25
R_2	0.1233	147.17	R_6	0.6297	105.88
R_3	0.3108	106.82	R_7	0.3946	106.87
R_4	0.5888	106.35	R_8	0.4505	107.53

3.3. Determination of optimal settings for proposed curve

In a LVDC microgrid with small line lengths and without optimal relay settings, maintaining appropriate coordination between relay pairs during LRF is crucial due to comparable $I_{rr,f_{iL}}$ and $I_{rr,f_{jL}}$. Line current rise rates of pair $R_3 - R_1$ for fault at F_4 in islanded mode of operation and pairs $R_2 - R_4$ for fault at F_1, $R_5 - R_3$ for fault at F_6 in radial configuration with GC mode of operation in Table 3 are a few such cases. More such cases can also be observed in Table 4. Further, for different network configurations, modes of operations, PG, PP LRFs and HRFs, the same set of relay pair may sense different line current rise rates, as evident from Tables 3 and 4. Additionally, line current rise rate of backup relay may be more than the same of primary relay as observed for relay pair $R_3 - R_1$ with fault at F_4 in islanded mode of operation in Table 4. Hence, various PG,PP LRFs, and HRFs are analyzed for different operating conditions with peak loads at buses in system of Fig. 2, as per notations defined in Table 7. The associated line current rise rates are already shown in Tables 3 and 4. The notations in Table 7 signify the M different scenarios in Section 2.2 and aid in compact representation of Fig. 3, Fig. 6–Fig. 9.

To obtain the proposed characteristic curve, A and γ in (8) are additional variables in Section 2.2, along with TMS_i and PS_i for each relay R_i in LVDC microgrid. As stated earlier, $B = 0$ in (8) to avoid unnecessary delay in relay operation. The values of $I^{min}_{rr,f_{iL}}$ and $I^{max}_{rr,f_{iL}}$ in Table 5 are used to obtain the single set of settings (TMS_i and PS_i) of each relay along with a common value of A and γ in (8), which can uphold appropriate coordination between primary-backup relay pairs for different faults and operating conditions of system in Fig. 2. The associated steps are as follows:

1. $\alpha_{(i/j)L,m}, \forall (i/j), \forall m \in M$ in (8), i.e., I_{rr,f_iL} and I_{rr,f_jL}, for relay pairs are taken for each scenario in Tables 3 and 4, as stated in Section 2.2.
2. The NLP-based proposed relay coordination problem, i.e., (4), (5), (7)–(14), is formulated next, where the associated bounds are evaluated as per Section 3.2.
3. The local minima of NLP is obtained from $fmincon$ which satisfies all constraints.
4. The obtained relay settings are validated for various LRFs and HRFs.

The obtained optimized values of A and γ in (8) for all operating conditions and relays in Fig. 2 are $0.037937 \approx 0.038$ and $1.5449 \approx 1.54$, respectively. The optimal unique TMS_i and PS_i for each relay R_i are given in Table 8. The obtained optimal value of z in (7) is 5.38 ms. A similar analysis is also done with $A^{max} = 100$ and $\gamma^{max} = 10$ in (13) and (14), respectively, to examine the effects of increase in A^{max} and γ^{max}. However, the new values of A and γ are 0.039 and 1.54, respectively, with $z = 5.378$ ms and similar values of TMS_i and PS_i are obtained, as reported in Table 8. This indicates that choosing $A^{max} \geq 1$ and $\gamma^{max} \geq 2$ in (13) and (14), respectively, has insignificant effect on the optimal relay settings. Hence, the rest of the analysis in this paper is done using $A = 0.038$ and $\gamma = 1.54$ in (8).

Table 9
Primary and backup relays' operating times, and associated difference in operating times in μs of relay pairs in Table 2 for scenarios in Table 3 and Table 4 (β - primary relay operating time, δ - backup relay operating time).

RPs	Ring						Radial		
	GC			Islanded					
	β	δ	$\delta-\beta$	β	δ	$\delta-\beta$	β	δ	$\delta-\beta$
				PG LRF (HRF)					
1	27.2(250.1)	100.1(960.4)	72.9(710.3)	27.9(236.2)	110.6(981.8)	82.7(745.6)	–	–	–
2	17.38(137.1)	139.4(1100)	122.0(962.9)	28.2(196.0)	171.4(1200)	143.2(1004)	15.9(117.5)	116.1(778.0)	100.2(660.5)
3	21.5(163.3)	104.5(800.8)	82.9(637.5)	28.4(191.4)	100.1(679.7)	71.7(488.2)	25.1(187.6)	142.1(1100)	117.0(912.4)
4	43.1(324.8)	149.2(1200)	106.1(875.2)	59.5(394.9)	134.2(906.5)	74.8(511.5)	43.9(330.0)	158.9(1200)	115.0(870)
5	15.9(121.1)	71.0(552.9)	55.1(431.8)	24.2(160.6)	82.1(551.9)	57.8(391.4)	15.5(116.3)	65.7(415.0)	50.2(298.7)
6	26.6(222.1)	87.7(751.7)	61.1(529.6)	27.1(218.9)	97.2(808.8)	70.1(589.9)	–	–	–
7	22.5(191.1)	93.8(900.1)	71.3(708.9)	23.9(197.6)	134.9(1300)	111(1102)	–	–	–
8	19.9(181.4)	69.9(718.1)	50.01(536.7)	21.6(189.3)	117.6(1300)	96.0(1111)	–	–	–
				PP LRF					
1	34.6	84.6	50.0	34.9	110.3	75.4	–	–	–
2	29.5	109.2	79.7	47.2	179.8	132.6	26.6	76.9	50.3
3	40.9	97.9	57.0	49.1	99.1	50.0	46.5	143.9	97.4
4	42.9	143.4	100.5	84.9	135.0	50.1	43.5	171.0	127.5
5	17.8	88.3	70.5	37.2	93.3	56.1	17.3	68.3	51.0
6	33.8	83.8	50.0	34.1	102.4	68.3	–	–	–
7	25.0	75.1	50.1	27.2	189.7	162.5	–	–	–
8	20.2	71.0	50.8	27.6	197.9	170.3	–	–	–

It can be noted that the settings in Table 8 for the proposed curve satisfy the bounds chosen for (4), (5) in Section 3.2. Further, these settings are validated next for different modes of operations, network configurations, LRFs, and HRFs for the considered test system in Fig. 2.

3.4. Validation of obtained settings for PG LRFs , PP LRFs and PG HRFs in Tables 3 and 4

The efficacy of the obtained optimal single settings, i.e., $A = 0.038$, $\gamma = 1.54$, TMS_i, and PS_i in Table 8, for the proposed relay characteristic curves is tested for coordination between the relay pairs in Table 2 for different modes of operations, network configurations, LRFs, HRFs while satisfying (9) and (10), as shown in Table 9 and Fig. 3. It can be observed from the second, fifth, and eighth columns of Table 9 that the minimum primary relay operating time is 15.5 μs (R_5 in fifth relay pair for scenario 'ag' in Table 7) while the maximum primary relay operating time is 394.9 μs (R_4 in fourth relay pair for scenario 'af'). Similarly, it can be noted from the third, sixth, and ninth columns of Table 9 that the minimum backup relay operating time is 65.7 μs (R_3 in fifth relay pair for scenario 'ag' in Table 7) while the maximum backup relay operating time is 1300 μs (R_5 and R_2 for scenario 'af'). These operating times satisfy the chosen bounds of (9) in Section 3.2, essentially fulfilling the quick line fault clearing requirement in LVDC microgrids. Also, it is evident from Fig. 3 that the difference in operating times of relays in Table 2 satisfy (10) for different scenarios in Tables 3 and 4. The proposed technique in Section 2 and associated analysis can be similarly extended to other LVDC microgrids with the difference being that the number of scenarios to be considered, i.e., M, will vary accordingly.

3.5. Validation of obtained settings for other faults in Fig. 2

The obtained optimal single settings, i.e., $A = 0.038$, $\gamma = 1.54$, TMS_i, and PS_i in Table 8, for the proposed relay characteristic curves are obtained considering the scenarios in Tables 3 and 4 so that the obtained settings can also effectively coordinate relay pairs in Table 2 for other possible line faults in Fig. 2, as discussed in Section 3.2. In order to test this aspect of the proposed scheme, relay pairs in Table 2 are tested for coordination using the obtained relay settings in Section 3.3 for following faults: PG with $R_f = 10\ \Omega$ and PP with $R_f = 1\ \Omega$ at 50% of all line lengths (one at a time) in Fig. 2 for GC (islanded) mode of operation. It is observed that with these optimal and unique settings, relay pairs in Table 2 have effective coordination, as the operating times of associated primary relays are in range of [127.6, 303.4] μs ([172.6, 381.8] μs) for PG fault and [42.99, 81.76] μs ([59.88, 131.91] μs) for PP fault in GC (islanded) mode of operation. These operating times satisfy the chosen bounds of (9) in Section 3.2. The same is also observed for the corresponding backup relays' operating times. Further, the obtained pair-wise difference in relays' operating times ($\delta - \beta$) is shown in Fig. 4, where it can be noted that the pair-wise difference of times in relay pairs satisfy the chosen bounds of (10) for these faults also.

Thus, by collectively analyzing Figs. 3 and 4, it can be concluded that the obtained optimal relay settings in Table 8 with $A = 0.038$ and $\gamma = 1.54$ in (8) effectively ensure relay coordination for all possible line faults in the considered LVDC microgrid of Fig. 2. These single settings also satisfy the quick line fault clearing requirement of LVDC microgrids.

3.6. Validation of obtained settings for intermittency in solar PV generation and other line outages in Fig. 2

The variation in line current rise rate due to the intermittent power generation from solar PV_1 source (solar irradiance varied from 1000 W/m^2 to 400 W/m^2) in Fig. 2 is observed here as given in Table 10. It can be noted from Table 10 that I_{rr} during a line fault does not vary significantly with varying irradiance. Also, the observed I_{rr} with varying irradiance in Table 10 are within the considered range of minimum and maximum I_{rr} in Table 5 to obtain the relay settings in the proposed work. Hence, the obtained relay settings with the proposed methodology hold true for these scenarios as well. Each relay pair positively satisfies the minimum CTI of 50 μs in Table 10, indicating that the obtained optimal relay settings are robust against intermittency of generation from renewable energy sources.

Similarly, to validate the obtained optimal settings of the relay under different network topologies, other line outage cases in Fig. 2 have been considered. As in Section 3.2, to obtain the optimal relay settings, an exhaustive analysis is done considering line L_{14} outage. Hence, to verify the obtained relay settings for other network topologies, we have analyzed the relay coordination for a close-in PG fault of $R_f = 0.01\ \Omega$ on line L_{23} during L_{12} outage and on line L_{12} during line L_{23} and L_{34} outages, as given in Table 11. It can be noted from Table 11 that I_{rr} with different line outages are within the considered range of minimum and maximum I_{rr} in Table 5 to obtain the relay settings in the

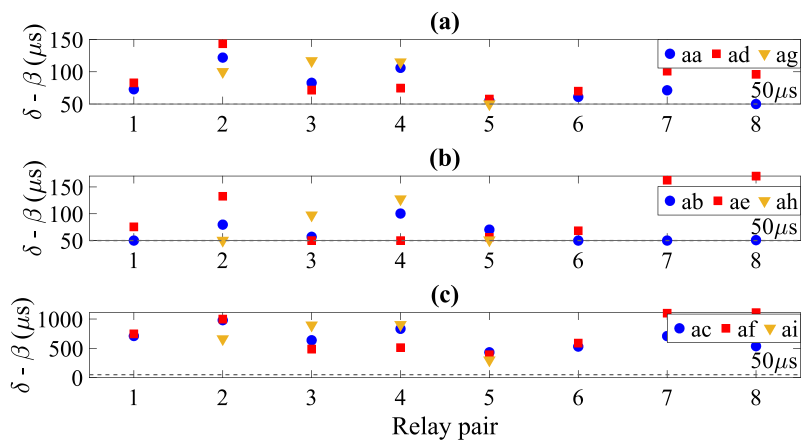

Fig. 3. Pair-wise difference in relay operating times for (a) PG LRFs, (b) PP LRFs, and (c) PG HRFs, in Table 9, as per Table 7.

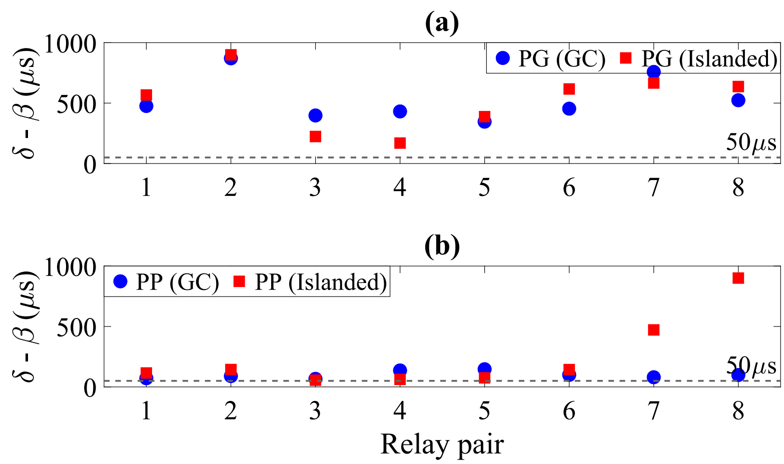

Fig. 4. Difference in relay operating times using settings from Section 3.3 for (a) PG (R_f = 10 Ω) and (b) PP (R_f = 1 Ω) faults in ring configuration of Fig. 2 (δ and β are primary and backup relay operating times, respectively).

proposed work. Hence, the obtained relay settings from the proposed methodology hold true for these scenarios as well. From Table 11, it can be inferred that each relay pair positively satisfies the minimum CTI of 50 μs. Thus, from the above analysis, it can be concluded that the obtained optimal relay settings in the proposed work are robust against intermittency of renewable energy sources and other network topologies with different line outages.

4. Comparative analysis

4.1. Comparison of proposed relay characteristic with SI and EI characteristics

Among several standard IEC/IEEE family of curves [18,19], SI and EI characteristics with respective characteristic constants $A = 0.14$, $B = 0$, $\gamma = 0.02$, and $A = 80$, $B = 0$, $\gamma = 2$ in (8) (irrespective of relay R_i and scenario m), are widely used for line protection in AC microgrids. Hence, the efficacy of these curves with the proposed curve are compared in a LVDC microgrid by observing the variations in corresponding relay operating times for $TMS = 0.01$s and $PMS \in [1.5, 20]$ as shown in Fig. 5.

It can be noted from Fig. 5(a) that the relay operating time for proposed curve with $A = 0.038$ and $\gamma = 1.54$ is in range of $[3.80, 438]$ μs. However, the relay operating times for SI and EI curves are in the range of $[23, 172]$ ms and $[2, 640]$ ms, respectively. Although the relay operating time with high PMS is less in EI curve compared to SI curve, the operating time in former is still high for LVDC microgrid line protection for chosen range of PMS. On the contrary, the relay operating time is very low (order of a few μs) for high PMS in proposed curve, making it preferable for LVDC microgrid protection. Further, for low PMS, the relay operating times in SI and EI curves are very high (order of hundreds of ms), while the same in proposed curve is low (order of hundreds of μs), as shown in Fig. 5(b). This indicates the capability of the proposed curve to provide protection against PG HRF in LVDC microgrid. Please note that the above analysis indicates the possible relay operating times for a particular relay using a particular characteristic curve (proposed, SI or EI), neglecting the required CTI satisfaction with respect to the backup relay, and the actuating quantity. In fact, PMS can be very different from 20 (the

Table 10
Line current rise rate for a close-in PG fault of R_f = 0.01 Ω on line L_{12} in Fig. 2 considering intermittent power generation of solar PV_1 source due to varying irradiance.

Irradiance (W/m²)	R_1 I_{rr}^{12}(pu/s)	R_7 I_{rr}^{41}(pu/s)	R_2 I_{rr}^{21}(pu/s)	R_4 I_{rr}^{32}(pu/s)
1000	8935.2 (28.17 μs)	2470.21 (207.53 μs)	2419.6 (63.69 μs)	841.72 (202.07 μs)
800	8982.4 (27.94 μs)	2482.67 (205.92 μs)	2439.47 (62.88 μs)	844.93 (200.8 μs)
600	8962.4 (28.04 μs)	2460 (208.87 μs)	2468.21 (61.75 μs)	861.2 (194.78 μs)
400	8925.19 (28.22 μs)	2458.67 (209.04 μs)	2432.93 (63.15 μs)	847.87 (199.72 μs)

Table 11
Line current rise rate for a close-in PG fault of $R_f = 0.01\ \Omega$ considering different line outages in Fig. 2.

Line outage	I_{rr}(pu/s)	I_{rr}(pu/s)	I_{rr}(pu/s)	I_{rr}(pu/s)
L_{12}	– –	– –	R_4(3964.51) (85.38 μs)	R_6(1223.54) (528.67 μs)
L_{23}	R_1(7989.6) (33.47 μs)	R_7(3213.33) (138.05 μs)	– –	– –
L_{34}	R_1(7472.47) (37.11mus)	R_7(2548.67) (197.7 μs)	R_2(2199.83) (73.91 μs)	R_4(621.08) (331.24 μs)

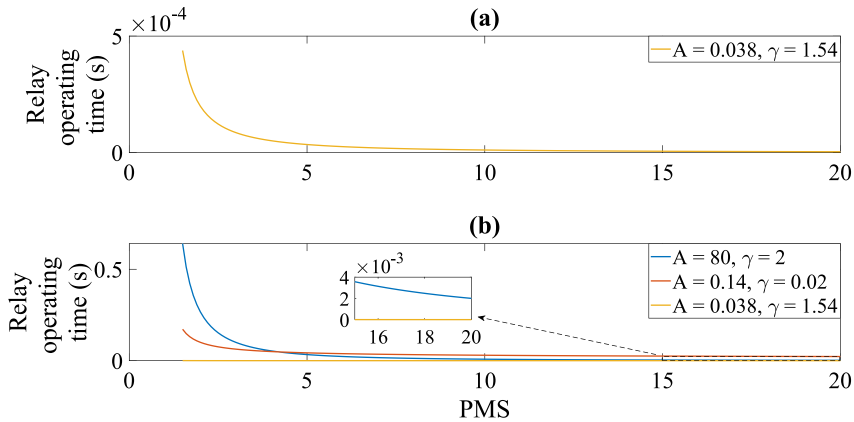

Fig. 5. (a) Proposed curve (b) EI, SI, and Proposed curves for $TMS = 0.01$s, $B = 0$, and $PMS \in [1.5, 20]$.

maximum PMS in Fig. 5) depending on the actuating quantity, PS, and system condition. Thus, the issues with using SI and EI curves in LVDC microgrid with line current and line current rise rate as actuating quantities are analyzed next.

4.2. Issues with SI and EI characteristic in LVDC microgrid relay coordination

4.2.1. Line current as actuating quantity

To analyze the feasibility of the SI and EI curves in LVDC microgrid with $\alpha_{iL,m}$ in (8) as the line current, (4), (5), (7)–(10) is solved with fixed characteristic constants (stated in Section 4.1). Similar to (11) and (12), appropriate bounds on $PS_i, \forall i$ based on steady-state and line fault currents are taken for like scenarios, as given in Table 7. The bounds on the relevant constraints are chosen as per the discussion in Section 3.2 with the optimization variables being $TMS_i, \forall i$ and $PS_i, \forall i$. It is observed that no feasible solution can be obtained for the above NLP problems. The reason for the infeasibility is the likely violation of (9) due to lower fault currents than the chosen lower bound of PS_i, especially for some PG HRF. Hence, it is possible that the above NLP problems with SI and EI curves having line current as actuating quantity may be feasible, provided a few specific fault scenarios, such as PG HRFs, are not considered, or the bounds on (4), (5), (9), (10), are relaxed, as discussed in Section 4.5. Also, in [16], the above conventional curves are used for line fault protection in DC microgrids with TMS_i in range of a few μs. However, setting a very low TMS_i may overshadow other characteristic parameters. Further, instantaneous or definite time relay characteristics may work in small DC radial systems, yet selective relay coordination becomes troublesome with increased number of buses and ring configuration.

4.2.2. Line current rise rate as actuating quantity

Depending on the fault type, line current rise rate in a DC microgrid may be several times more than the nominal value, as observed in Tables 3 and 4, essentially resulting in high PMS. The applicability of conventional SI and EI curves in LVDC microgrid relay coordination is also analyzed with line current rise rate as actuating quantity considering all scenarios in Table 7. It is observed that no feasible solution exists for the associated NLP, i.e., (4), (5), (7)–(12), for SI curve, which is likely due to the violation of (9) (similar to Section 4.2.1). Further, as per (2) and (8), the relay time for SI curve is minimum when the associated TMS and PS are at their lower bounds (chosen in Section 3.2). However, it can be observed from Fig. 6 that the minimum calculated relay operating times are more than the chosen upper bound on relay operating time in (9), i.e., $t_{o_i}^{\max} = 5ms, \forall i$ in Section 3.2. This further justifies the infeasibility of associated NLP for SI curve with line current rise rate as actuating quantity in Fig. 2.

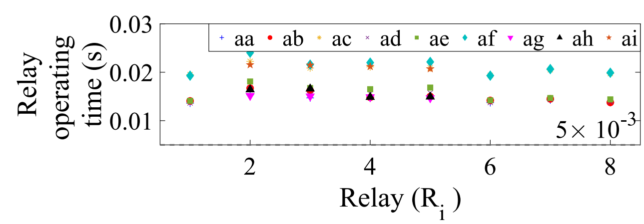

Fig. 6. Calculated primary relay time for SI curve with TMS_i and PS_i are lower bounds (chosen in Section 3.2) for scenarios defined in Table 7.

A similar analysis is also done for the EI curve, and a local minima is obtained with $z = 0.0409$s in (7). The obtained TMS_i and PS_i settings are given in Table 12, where it can be noted that most TMS_i and PS_i values are close to their lower bounds. Further, the observed pair-wise difference in relay operating times and primary relay operating time with settings from Table 12 are shown in Fig. 7. It can be observed from Fig. 7 that the maximum primary relay operating time is 2.78 ms, contrary to 394.9 μs for proposed curve with $A = 0.038$ and $\gamma = 1.54$. Also, the maximum primary relay operating time for EI curve is close to the upper bound of (9).

Thus, from the above analysis, it can be concluded that the conventional EI curve has better applicability than the SI curve in an LVDC microgrid for considered constraints, i.e., (4), (5), (8)–(12). However, the very low objective value and significantly low primary relay operating time of the proposed curve than the EI curve, especially for PG HRF, indicate the superiority of utilizing the proposed curve in a LVDC microgrid, even for PG HRF.

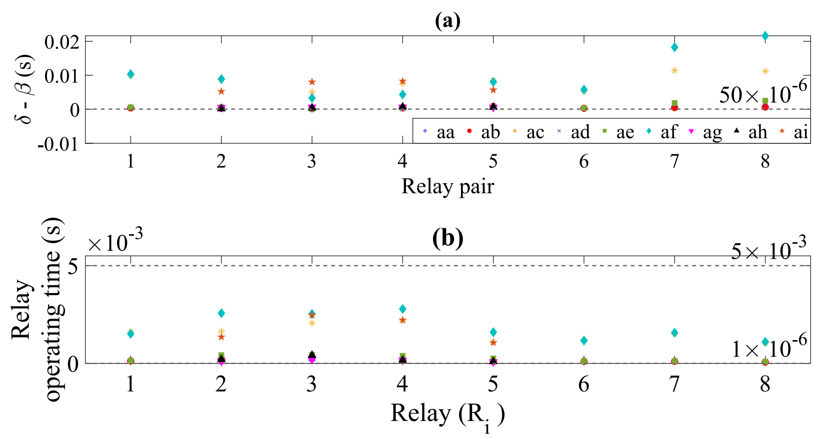

Fig. 7. Obtained (a) pair-wise difference in relay times ($\delta - \beta$) and (b) primary relay time for EI curve with line current rise rate as actuating quantity.

Table 12
Obtained single settings of relays in Fig. 2 for conventional EI curve with line current rise rate as actuating quantity.

R_i	TMS_i (s)	PS_i	R_i	TMS_i (s)	PS_i
R_1	0.0203	68.109	R_5	0.0100	67.114
R_2	0.0100	66.670	R_6	0.0110	81.716
R_3	0.0172	66.671	R_7	0.0140	66.673
R_4	0.0100	86.297	R_8	0.0120	66.911

4.3. Issues with using line current as actuating quantity in proposed curve

The efficacy of using line current as an actuating quantity in the proposed characteristic curve is also tested. For this, (4), (5), (7)–(10) with appropriate bounds on $PS_i, \forall i$ based on line currents, similar to (11), (12), is solved considering similar scenarios as in Table 7 while utilizing steady-state and line fault currents of the considered microgrid in Fig. 2. The bounds on relevant constraints are chosen as per Section 3.2 with the optimization variables being A, γ, $TMS_i, \forall i$ and $PS_i, \forall i$. Additionally, bounds on A and γ are chosen as $[0.01, 100]$ and $[0.001, 100]$, respectively. However, due to significantly low fault current during PG HRF, no feasible solution is obtained, which indicates that line current is not a suitable actuating quantity in the proposed curve.

4.4. Comparison with [16]

To prove the efficacy of the proposed work, the test system of [16] has also been modeled in RTDS as shown in Fig. 8 and the associated optimal relay settings have been obtained using the proposed novel relay characteristic discussed in Section 2.2. The relay settings for the test system shown in Fig. 8 are determined by considering various close-in and line-end PG, PP LRFs ($R_f = 0.01\ \Omega$), and PG HRFs ($R_f = 20\ \Omega$) in lines of DC microgrid for the given peak load in [16] at each bus. 400 V and 250 A are considered as the base quantities. Similar to the study done in Section 3.2, here $I_{rr_i}^{nom}$ is calculated as 16 pu/s for each relay. Further, PS_i^{min} and PS_i^{max} are determined by performing a comprehensive PG and PP LRFs and PG HRFs analysis at fault locations F_L (F_1, F_2, F_3, and F_4) in Fig. 8, as given in Table 13.

Substituting $I_{rr_i}^{nom}$ = 16 pu/s, and minimum and maximum line current rise rate from Table 13, and using SF = 1.25 in (11), (12), the bounds on PS_i for each relay in Fig. 8 are $PS_i^{min} = 20\ \forall\ R_i$ and PS_i^{max} as 3729.92, 11264.8, and 13348.6 for relay R_1, R_2, and R_3, respectively.

Further, the optimal relay settings are obtained by choosing bounds on TMS_i^{min}, TMS_i^{max}, t_{oi}^{min}, t_{oi}^{max}, CTI_i, A and γ, similar to the discussion in Section 3.2. The obtained optimized values of A and γ for all relays in Fig. 8 are $0.010007 \approx 0.01$ and $1.0078 \approx 1.01$, respectively. The optimal unique TMS_i and PS_i for each relay R_i are given in Table 14. The primary and backup relays' operating times in μs using obtained optimal settings of relays for scenarios in Table 13 are given in Table 15.

Table 13
Line current rise rate in pu/s sensed by relays at different F_L in Fig. 8.

F_L	R_i	PG LRF	PG HRF	PP LRF
F_1	R_2	11 264.8	801.57	8657.82
	R_1	3729.92	263.779	3552.62
F_2	R_2	7483.12	547.23	5381.21
	R_1	3096.89	261.81	3452.62
F_3	R_3	13 348.6	967.01	9477.21
	R_2	6035.39	629.58	5506.86
F_4	R_3	9907.11	800.62	6632.38
	R_2	5776.12	486.49	5358.83

Table 14
Obtained optimal settings of relays in Fig. 8 for the proposed curve.

R_i	$TMS_i(s)$	PS_i
R_1	0.83962	89.922
R_2	0.99468	35.883
R_3	0.50031	20.012

Table 15
Primary and backup relays' operating times in μs for scenarios in Table 13.

F_L	R_i	PG LRF	PG HRF	PP LRF
F_1	R_2	30.40	454.74	40.09
	R_1	201.45	4300	211.84
F_2	R_2	45.98	682.73	64.23
	R_1	244.19	4321	218.18
F_3	R_3	7.143	102.57	10.09
	R_2	57.18	587.47	62.74
F_4	R_3	9.65	124.61	14.48
	R_2	59.78	775.38	64.51

To compare the proposed novel relay coordination technique with the methodology in [16] and to validate the obtained relay settings for the relays in Fig. 8, similar to [16], a PG fault with $R_f = 0.1\ \Omega$ at bus B_4 is analyzed. The line current rise rate observed by R_3 and R_2 for PG fault with $R_f = 0.1\ \Omega$ at bus B_4 are 9869.32 pu/s and 5371.75 pu/s, respectively. The operating time of the primary relay R_3 for PG fault with $R_f = 0.1\ \Omega$ at bus B_4 with the proposed technique is 10.12 μs, which is much lesser than the reported operating time (> 50 μs) in [16]. Similarly, the operating time of the backup relay R_2 is observed as 66.67 μs, positively satisfying the CTI_i^{min} of 50 μs. It is to be noted that in [16], TMS for relays in the range of few μs, which may undermine the significance of other parameters of the used curve.

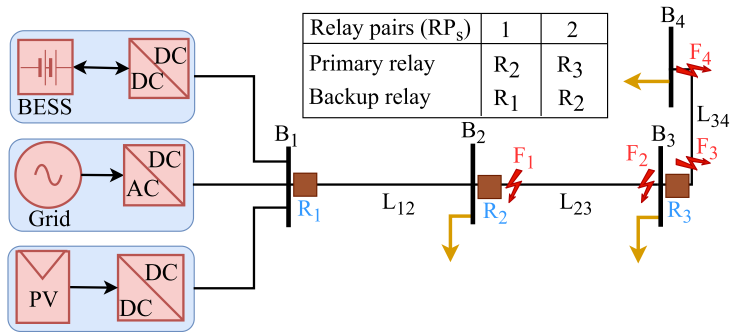

Fig. 8. 400-V grid-connected DC microgrid test system [16].

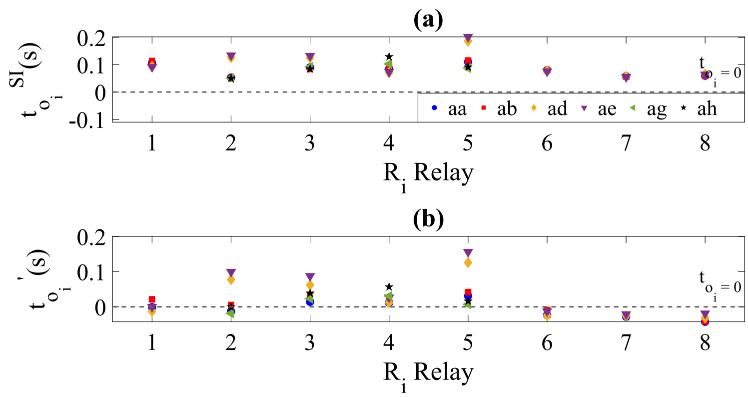

Fig. 9. (a) $t_{o_i}^{SI}$ (b) t'_{o_i} for [17], using settings of Table 16.

Table 16
Obtained TMS and PS settings for relays in Fig. 2 for [17].

R_i	TMS_i (s)	PS_i	R_i	TMS_i (s)	PS_i
R_1	0.0153	1.176	R_5	0.0162	0.872
R_2	0.0130	0.622	R_6	0.0108	1.399
R_3	0.0145	1.160	R_7	0.0102	0.753
R_4	0.0116	0.696	R_8	0.0107	0.842

4.5. Comparison with [17]

In [17], successive current difference ($\Delta I_k = I_k - I_{k-1}$) of line current is used to obtain low relay operating time (t_{o_i}) and a better boundary between primary and backup relay using $t'_{o_i} = t_{o_i}^{SI} - \beta \times (\Delta I_k)$. In this expression, $t_{o_i}^{SI}$ is the operating time of relay R_i using conventional SI curve having current as actuating quantity, t'_{o_i} is the operating time of the same R_i with the incorporation of $\beta \times (\Delta I_k)$. β is a factor to regulate the implication of ΔI_k on t'_{o_i}. It is reported in [17] that $t_{o_i}^{SI}$ is of the order of a few ms. Hence, considering the reported range of $t_{o_i}^{SI}$ in [17] and the issues with using SI curve with line current as actuating quantity in Section 4.2.1, all scenarios in Table 7, except the PG HRFs, are considered to obtain TMS and PS settings for [17]. Additionally, the upper bound on relay operating time ($t_{o_i}^{SI}$ in [17]) in (9) is increased to 1s, while (4), (5), (7), (8), (10)–(12) remain the same as in Section 4.2.1. The associated obtained values of TMS_i and PS_i for each relay R_i in Fig. 2 in this case are given in Table 16. The associated $t_{o_i}^{SI}$ and t'_{o_i} are shown in Fig. 9.

It can be inferred from Fig. 9(a) and Fig. 9(b) that by using $\beta\times(\Delta I_k)$, the maximum $t_{o_i}^{SI}$ = 201 ms is reduced to t'_{o_i} = 156 ms, while the maximum primary relay operating time with the proposed curve is 84.9 μs for LRFs. Further, the value of β in $t'_{o_i} = t_{o_i}^{SI} - \beta\times(\Delta I_k)$ is crucial, as t'_{o_i} may become negative, when $\beta\times(\Delta I_k)$ dominates $t_{o_i}^{SI}$, as observed for some cases in Fig. 9(b). Thus, a comparison of Fig. 9 and Fig. 3 indicates that the proposed technique is superior to [17] in terms of obtaining single optimal relay settings for all faults, including HRFs, and operating conditions of LVDC microgrid.

5. Conclusion

This paper proposes a novel inverse time relay characteristic for the protection of DC microgrids against line faults using line current rise rate as an actuating quantity. It can coordinate relays in a DC microgrid with non-unit fault detection schemes or act as a backup scheme for relays with communication-based primary method. The relay coordination using the proposed characteristic is tested on a 400V LVDC microgrid. A single set of optimal relay settings (TMS_i and PS_i) and a common set of values of A and γ in (8) are obtained, considering all possible modes of operation, network configurations, and worst-case PG, PP LRFs and PG HRFs. Consequently, the proposed approach does not require an online update of TMS_i and PS_i with a change in operating condition of DC microgrid. The efficacy of the proposed curve is validated with the obtained optimal unique relay settings for various PG, PP LRFs, PG HRFs for GC, islanded modes of operation, ring, radial network configurations, and intermittency of generation from renewable energy sources. Zero relay miscoordinations with a maximum primary relay operating time with the proposed curve are 84.9 μs and 394.9 μs for LRF and HRF faults, respectively, proving the effectiveness of the proposed technique in LVDC microgrid.

Further, the issues of using SI and EI curves to coordinate relays in a LVDC microgrid using line current and line current rise rate as actuating quantity and issues with using line current as actuating quantity in proposed scheme are discussed. It is observed that the conventional EI curve with line current rise rate may be used for relay coordination in DC microgrid. However, the high relay operating time (maximum primary relay operating time being 2.78 ms) may lead to prolonged line fault isolation. Additionally, the proposed scheme is fast and reliable, compared to EI curves, since the sum of primary relay operating times, considering all fault scenarios, is 5.38 ms with the proposed curve, compared to the EI curve, which gives 40.9 ms. The comparison with [16,17] reveals the efficacy of the proposed scheme with the relay operating times in the proposed scheme being in the range of a few μs for line faults in LVDC microgrid.

CRediT authorship contribution statement

Sunil Kumar Maurya: Conceptualization, Methodology and formulation, Software, Data curation, Writing – original draft, Visualization, Investigation, Validation. **Atul Kumar Soni:** Visualization, Investigation, Formulation. **Abheejeet Mohapatra:** Supervision, Writing – review & editing. **Ankush Sharma:** Supervision, Writing – review & editing.

Declaration of competing interest

The authors declare that they have no known competing financial interests or personal relationships that could have appeared to influence the work reported in this paper.

Data availability

No data was used for the research described in the article.

References

[1] Elsayed AT, Mohamed AA, Mohammed OA. DC microgrids and distribution systems: An overview. Electr Power Syst Res 2015;119:407–17.
[2] Naik J, Dhar S, Dash P. Adaptive differential relay coordination for PV DC microgrid using a new kernel based time-frequency transform. Int J Electr Power Energy Syst 106:56–67.
[3] Farhadi M, Mohammed O. Adaptive energy management in redundant hybrid DC microgrid for pulse load mitigation. IEEE Trans Smart Grid 2015;6(1):54–62.
[4] Shamsoddini M, Vahidi B, Razani R, Mohamed YA-RI. A novel protection scheme for low voltage DC microgrid using inductance estimation. Int J Electr Power Energy Syst 2020;120:105992.
[5] Wang T, Chu X, Hussain KST, Gao J. Fault control and line protection strategy for LVDC microgrids based on modified high-frequency-link DC solid state transformer. Int J Electr Power Energy Syst 2022;140:108052.
[6] Kim S, Ulissi G, Kim S-N, Dujic D. Protection coordination for reliable marine DC power distribution networks. IEEE Access 2020;8:222813–23.
[7] Rodrigues R, Du Y, Antoniazzi A, Cairoli P. A review of solid-state circuit breakers. IEEE Trans Power Electron 2021;36(1):364–77.
[8] Feng Y, Zhou Y, Shen ZJ. SiC solid state circuit breaker with an adjustable current-time tripping profile. In: 2018 IEEE applied power electron. conf. expo. 2018, p. 1968–73. http://dx.doi.org/10.1109/APEC.2018.8341287.
[9] Shabani A, Mazlumi K. Evaluation of a communication-assisted overcurrent protection scheme for photovoltaic-based DC microgrid. IEEE Trans Smart Grid 2020;11(1):429–39.
[10] Qi L, Cairoli P, Pan Z, Tschida C, Wang Z, Ramanan VR, et al. Solid-state circuit breaker protection for DC shipboard power systems: breaker design, protection scheme, validation testing. IEEE Trans Ind Appl 2020;56(2):952–60.
[11] Hill JE, Fletcher SD, Norman PJ, Galloway SJ. Protection system for an electrical power network. 2012, U.S. Patent Application US 20120200966 A1.
[12] Yang J, Fletcher JE, O'Reilly J. Short-circuit and ground fault analyses and location in VSC-based DC network cables. IEEE Trans Ind Electron 2012;59(10):3827–37.
[13] Feng X, Qi L, Pan J. A novel fault location method and algorithm for DC distribution protection. IEEE Trans Ind Appl 2017;53(3):1834–40.
[14] Langston J, Schoder K, Sloderbeck M, Steurer M, Rockhill A. Testing operation and coordination of DC solid state circuit breakers. In: 44th annual conf. IEEE ind. electron. soc. 2018, p. 3445–52.
[15] Rachi MRK, Khan MA, Husain I. Local measurement-based protection coordination system for a standalone DC microgrid. IEEE Trans Ind Appl 2021;57(5):5332–44. http://dx.doi.org/10.1109/TIA.2021.3091945.
[16] Kheirollahi R, Zhao S, Zhang H, Lu X, Wang J, Lu F. Coordination of ultrafast solid-state circuit breakers in radial DC microgrids. IEEE J Emerging Sel Top Power Electron 2022;10(4):4690–702. http://dx.doi.org/10.1109/JESTPE.2021.3109483.
[17] Kaisar Rachi MR, Akhter Khan M, Husain I. Current derivative assisted protection coordination system for faster fault isolation in a radial DC microgrid. In: 2020 IEEE energy convers. congress exp. 2020, p. 1292–8.
[18] Benmouyal G, Meisinger M, Burnworth J, et al. IEEE standard inverse-time characteristic equations for overcurrent relays. IEEE Trans Power Delivery 1999;14(3):868–72.
[19] ALSTOM (Firm). Network protection and automation guide: protective relays, measurement and control. Alstom Grid; 2011.
[20] Meghwani A, Gokaraju R, Srivastava SC, Chakrabarti S. Local measurements-based backup protection for DC microgrids using sequential analyzing technique. IEEE Syst J 2020;14(1):1159–70. http://dx.doi.org/10.1109/JSYST.2019.2919144.
[21] Meghwani A, Srivastava SC, Chakrabarti S. A non-unit protection scheme for DC microgrid based on local measurements. IEEE Trans Power Delivery 2017;32(1):172–81. http://dx.doi.org/10.1109/TPWRD.2016.2555844.
[22] Maurya SK, Panda RK, Mohapatra A, Sharma A. $\Delta V - \Delta I$ Plane-based line faults detection and classification in DC microgrid. IEEE Trans Power Delivery 2022;1–12. http://dx.doi.org/10.1109/TPWRD.2022.3222876.
[23] URL https://tinyurl.com/bdzye3e3.
[24] Soni AK, Kumar A, Panda RK, Mohapatra A, Singh SN. Adaptive coordination of relays in AC microgrid considering operational and topological changes. IEEE Syst J 2023;17(2):3071–82. http://dx.doi.org/10.1109/JSYST.2022.3227311.
[25] Bedekar PP, Bhide SR. Optimum coordination of directional overcurrent relays using the hybrid GA-NLP approach. IEEE Trans Power Delivery 2011;26(1):109–19.
[26] Gers JM, Holmes EJ. Protection of electricity distribution networks. Energy engineering, IET; 2011.
[27] URL https://www.batteryspace.com/prod-specs/pl383562.pdf.
[28] Choudhary V, Hegarty T, Pace D. Under the hood of a non-inverting buck-boost converter. In: Power supply design seminar, no. 17. 2016.
[29] Tashakor N, Khooban M-H. An interleaved bi-directional AC–DC converter with reduced switches and reactive power control. IEEE Trans Circuits Syst II Express Briefs 2019;67(1):132–6.
[30] Dragičević T, Lu X, Vasquez JC, Guerrero JM. DC microgrids—Part II: A review of power architectures, applications, and standardization issues. IEEE Trans Power Electron 2016;31(5):3528–49.